8. ADVANCED ACOUSTIC TECHNIQUES FOR HEALTH MONITORING OF CONCRETE STRUCTURES

Dimitrios G. AGGELIS, Theodore E. MATIKAS and Tomoki SHIOTANI

Summary

Contemporary engineering applications require materials with high toughness and durability. The safe infrastructure management calls for time- and cost- effective as well as global characterization techniques. Acoustic methods offer many advantages in that they are non invasive and can be applied during the normal service of the structure without interruption. The information obtained is related to the geometric location of the damaged zones and the severity of the condition. Current research aims to standardize the procedure of concrete Acoustic Emission testing and analysis in order to be reliably applied for in-situ monitoring. Acoustic emission indices can be used to predict final failure and characterize between different cracking modes enabling maintenance decisions based on robust engineering criteria. In the chapter, the basics of acoustic emission are described along with advanced indices and parameters, the validity of which is supported by experiments and simulation.

Keywords: Acoustic emission; Cracks; Infrastructure; Non Destructive Inspection.

8.1 INTRODUCTION

The aging of civil infrastructure calls for immediate and effective Non Destructive Evaluation (NDE) techniques. Information on the structural integrity, estimation of remaining strength, evaluation of the damage type and content can be considered in a process of safe and economic infrastructure management. Concerning large concrete structures, it is not always possible to determine the exact integrity condition of the whole volume. Still, NDE results can act as a warning before the structure deteriorates to a critical degree endangering human lives. Due to the large cost of building new infrastructure, the engineering community grows a standard interest on repair of existing structures with the aim of extending the safe service life of the structures for decades. Therefore, inspection methods which enable engineering decisions based on specific criteria are highly sought. These inspection methods should be global, reliable as well as time- and cost-effective.

The term "global" refers to the assessment of the largest possible volume of the material in one testing. Consequently, some specific parts of the structure can be targeted by more detailed pin-point inspection methods, in case it is deemed necessary.

Additionally, the results of the methods should be reliable and lead with little or no doubt to the correct conclusion concerning the structural integrity and consequently to the further steps of repair action. Therefore, certain procedures should be followed concerning the application of the method, as well as establishment of specific sensitive indices measured in a non destructive way with the capability to characterize the damage status of the structure. In case these features can be achieved by a testing method which can also be relatively cheap and fast, a large number of old structures can be scanned and prioritized concerning their risk assessment, something that will significantly contribute to the safe and economic infrastructure management. This is a field concentrating the effort of the engineering community, and different scientific committees are active investigating the standardization of NDE methods in concrete [8.1,8.2].

Methods based on elastic waves have proven very useful in several cases of monitoring and repair of large structures. These methods include both active (ultrasonic testing, UT) as well as passive techniques (acoustic emission, AE). In the first case, an excitation is introduced at several specific points of the structure [8.3, 8.4]. This propagates as an elastic wave through the material of the structure and can be received by suitable transducers at different points. Characteristics of the transient pulse, such as velocity and attenuation can provide useful insight of the interior's condition, visualize defects, as well as correlate with the elasticity modulus and strength of the material. Pulse velocity has been correlated with mix composition [8.5, 8.6] strength [8.7, 8.8] and damage [8.9-8.11] of concrete materials, offering rough but valuable estimations, since the damage condition influences the mechanical properties and hence wave speed and attenuation. Employing a number of sensors, the velocity structure of the material can be constructed and the internal condition visualized, highlighting the existence of voids or cracks, [8.12-8.14].

On the other hand, Acoustic Emission (AE) utilizes the transient waves which are emitted by the initiation and propagation of cracks when the material is under stress, hence there is no external trigger [8.15]. These transient waves (AE signals) are detected by AE sensors attached to the surface of the material, (in a general case they operate in a similar way to the UT sensors). The source of the transient signals is an AE "event" that is related to the fracture process (e.g. one crack nucleation or propagation incidence). One event leads to a stress wave propagating in all directions which is recorded almost simultaneously by different sensors. Analysis of the wave characteristics and the origin can provide useful information about the internal condition of the structure. The advantage of AE is the recording of the damage process during the entire load history, which enables determination of the onset of fracture and tracking of all subsequent failure stages. In several studies AE parameters have been correlated with the failure modes and damage evolution under bending test [8.16-8.20], pull out [8.21, 8.22] and splitting tests [8.23], even cracking due to drying shrinkage of fresh concrete [8.24]. Specific AE indices have been used to identify the moment of critical failures much earlier than visual observation or drop of mechanical load readings [8.25, 8.26]. Therefore AE is

employed in the monitoring of full scale structures like bridges [8.27], railway concrete piles [8.28, 8.29], dams [8.30] and land slide monitoring [8.31, 8.32].

8.2 ACOUSTIC EMISSION

The first referenced application of acoustic emission was thousands of years ago, when pottery manufacturers listened to the audible sounds from pots that had been cooled off more quickly than others. The pots that emitted this cracking sound were of lower quality and would fail before serious usage [8.33]. One of the first systematic examinations of AE was conducted by Kaiser at 1950s. It was observed that acoustic emission would be detected only after the previous maximum load had been overpassed [8.34]. Materials which are relatively intact follow the "Kaiser effect", while as damage is being accumulated acoustic emission emerges even at lower stress levels.

In general, acoustic emission can be defined as transient elastic waves which are generated by the release of energy mainly due to crack initiation and propagation incidences in a material [8.35]. Acoustic emission, which occurs in most materials, is caused by irreversible changes, such as dislocation movement, phase transformations, crack initiation, and propagation, debonding between continuous and dispersed phases in composite materials, corrosion and others [8.36-8.40]. In AE testing, the minor events created by slight fracture incidents are especially targeted in order to act as a precursor of the large scale fracture that could be catastrophic. AE signals (which are similar to the seismic activity of the Earth's crust but in a smaller scale) can be recorded by suitable sensors attached on the surface of the material. In a typical case the AE sensors are piezoelectric, transforming the pressure applied on their surface under the transient excitation of the AE signal to electrical voltage. For concrete applications the resonant frequency of the sensors is usually below 200 kHz for in-situ application [8.16, 8.28-8.30], while in laboratory when attenuation is not an issue due to reduced size of specimens more broadband sensors can be used.

A schematic representation of the AE testing technique is depicted in Figure 8.1. The normal sequence of the procedure includes the stressing of the examined material or structure. This could be a controlled experiment in laboratory conditions in order to examine the AE behavior during the fracture process within a material under monotonic or fatigue loading. In case of in-situ monitoring the stress is applied by the service load of the structure, (e.g. traffic on a bridge). Consequently, fracture phenomena (or

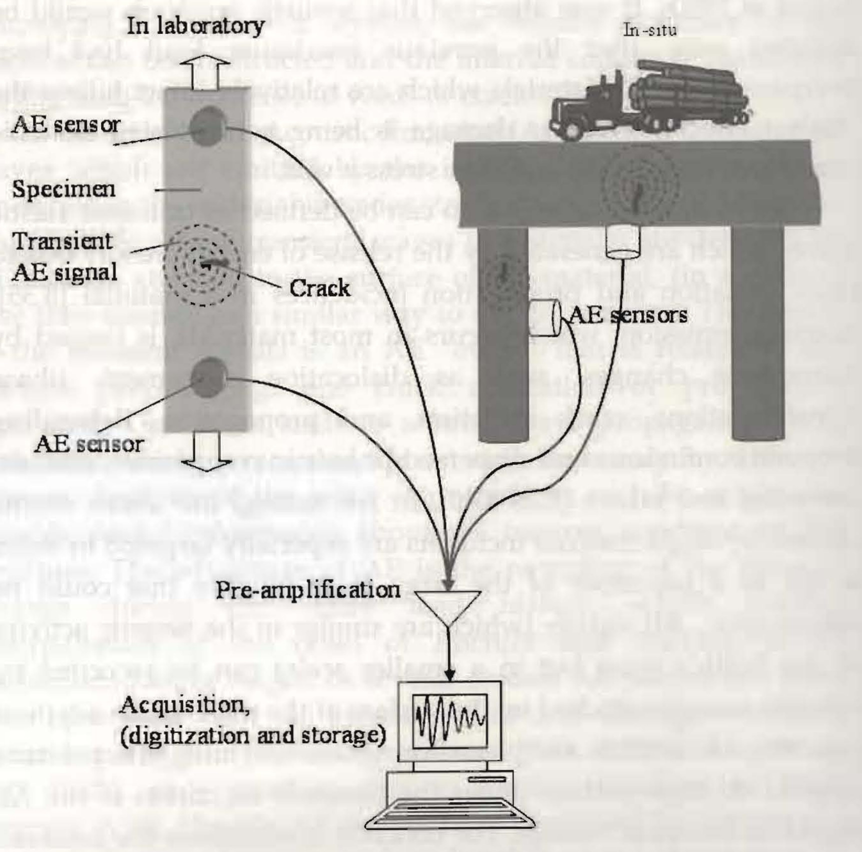

Figure 8.1 Typical acoustic emission procedure in laboratory and in-situ.

friction between already formed cracks sides) emerge and release transient elastic waves which propagate from the source crack as elastic waves. They are detected by the sensors attached on the surface, in the form of AE waveforms. These waveforms are digitized and stored in order to be analyzed. Most of the characteristics however, such as the total activity, AE signal parameters or the location of the sources can be seen on the screen in real time.

Considering that the acoustic activity depends on the number of crack propagation incidences, the hit rate can supply information about the activity of cracks. Under the same testing and loading conditions, high activity indicates increased rate of crack propagation events, while lower is connected to negligible crack intensity. Figure 8.2a shows an example of cumulative acoustic emission activity during a triangular loading cycle of a coupon of composite material [8.41]. Acoustic emission hits are being recorded from the start of the cycle but the rate starts to increase when load reaches half of the maximum. Seconds later, when the load decreases, AE activity rate reduces but hits are still recorded even during unloading. In certain materials, like reinforced polymers or metals used for pressure vessels or pipes, experience has indicated certain values of AE activity to be used as thresholds between intact, questionable and damaged material [8.42, 8.43]. However, due to the severe inhomogeneity of concrete, similar standards have yet to be defined.

Apart from the number of acoustic events, valuable information concerning the location of the cracks can be exploited. Considering that a number of AE sensors are located in the near vicinity of a crack tip, each one will record a signal (hit), which originates from the cracking event. In case the sound velocity of the medium is known, the relative delay between acquisition by the different sensors will depend on the actual location of the source crack. Therefore, using back-calculation algorithms, geometric location of the cracks is possible [8.16, 8.17, 8.21, 8.24, 8.44]. For a small tensile coupon of material, two sensors are enough to produce "linear" location, while for three dimensional location, at least six sensors are necessary. An example is seen in Figure 8.2b, where linear

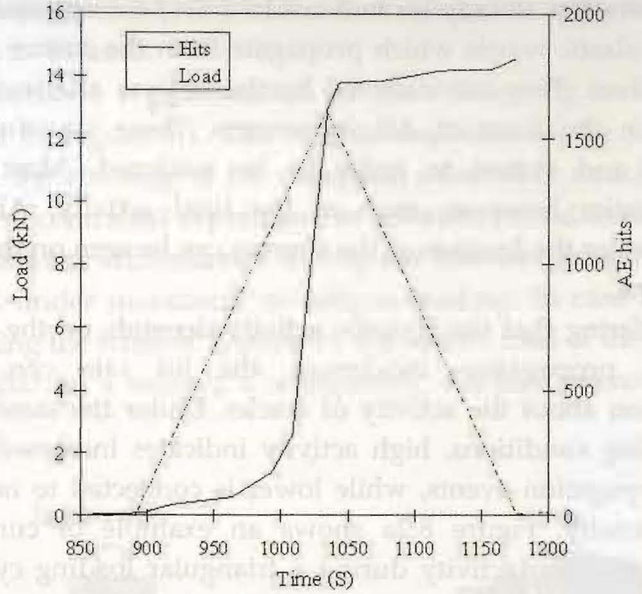

(a)

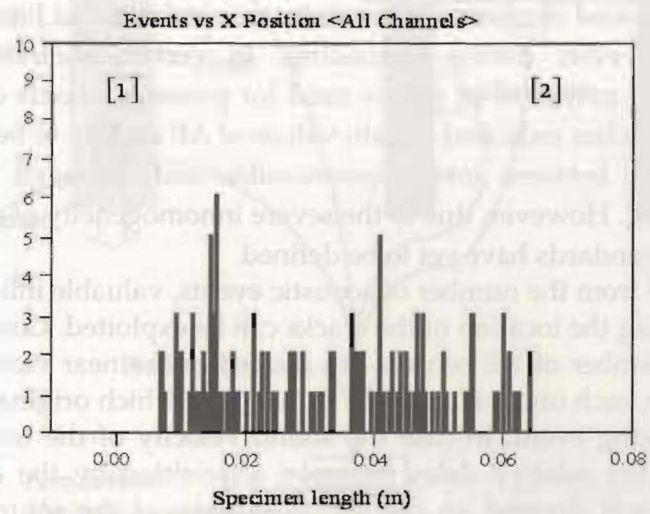

(b)

Figure 8.2 (a) Typical cumulative AE activity vs. load and time for a composite specimen, (b) linear location of AE events in a span of 70 mm in a specimen.

location on a 70 mm span of a composite specimen shows the crack density at specific locations. AE location indicates which part of the structure/specimen has suffered extensive deterioration and leads to specific action, like cement injection for a large concrete structure.

As stated earlier, when a material or structure is stressed, AE is produced. Additionally, the behavior during unloading is also crucial. In the case where the material is intact or the applied load is low, the AE activity during unloading is of low intensity, as seen in Figure 8.3. For damaged material though, the emissions are intense even during unloading, see again Figure 8.3. The number of AE events during unloading divided by the number of events during the whole cycle is defined as the calm ratio (CR) and values near 0 indicate intact material condition, while higher than 0.05 imply questionable quality [8.16, 8.27-8.29, 8.45, 8.46].

The parameters can be considered as quantitative, since they depend only on the sensitivity of the AE system to acquire signals. Source location and accumulated hit activity can be monitored regardless of the qualitative characteristics and shape of the acquired waveforms. Information based on the shape of each signal is also crucial to characterize the damage mode and intensity, but first two examples of large structures AE monitoring based on the number and the location of the events are presented.

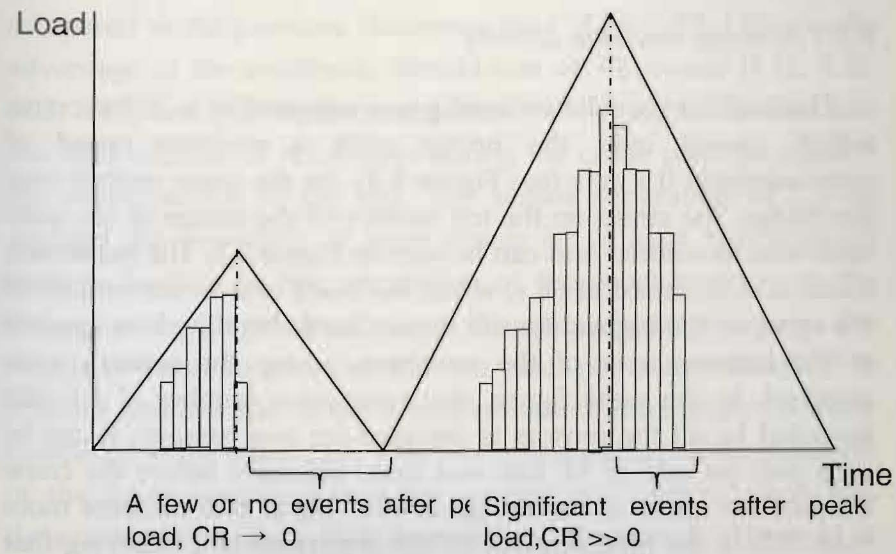

Figure 8.3 Representation of AE activity with damage process.

8.3 AE MONITORING OF A PRE-STRESSED CONCRETE BRIDGE

As an example of linear event location in a large structure the case of a prestressed concrete bridge is described along with some important details [8.13]. The length of the examined spam was 45 m. Due to the elongated shape of the structure the sensors were placed in one line along the center longitudinal axis of the bridge. The 28 sensors (R6 from Physical Acoustics Corp. (PAC)) were attached to the bottom surface of the bridge using electron wax. Their separation was 1.5 m. The approximate positions are shown in Figure 8.4. The R6 sensor has a resonant frequency of approximately 60 kHz and is widely used for concrete. Before the test, pencil lead breaks were performed near each sensor and the results were within 1 dB margin at the top of the voltage range, showing that all transducers were adequately mounted. The detected AE signals were pre-amplified by 40 dB and acquired in two synchronized data acquisition systems, namely a 16-channel DiSP and a 12-channel Mistras of PAC. Strain gauges were also placed in three locations of the top surface of the bridge, as shown in Figure 8.4.

8.3.1 Acoustic emission activity

The load for the AE monitoring was supplied by a 20-ton crane, which passed over the bridge with a constant speed of approximately 0.5 m/s (see Figure 8.4). As the crane moved over the bridge, the strain on the top surface of the bridge at the mid-span was monitored and can be seen in Figure 8.5. The maximum strain was recorded at 88 s, when the truck was in the middle of the span, as the highest tensile stress due to bending was applied at the bottom layer of the structure, where the sensors were attached. In the same figure, the cumulative number of AE hits recorded by all the sensors is depicted for one passage. It can be seen that the rate of AE hits was more intensive before the crane reached the center of the bridge at 88 s. Up to that moment more than 70% of the total number of hits was recorded, implying that more active sources were located in the first half of the bridge.

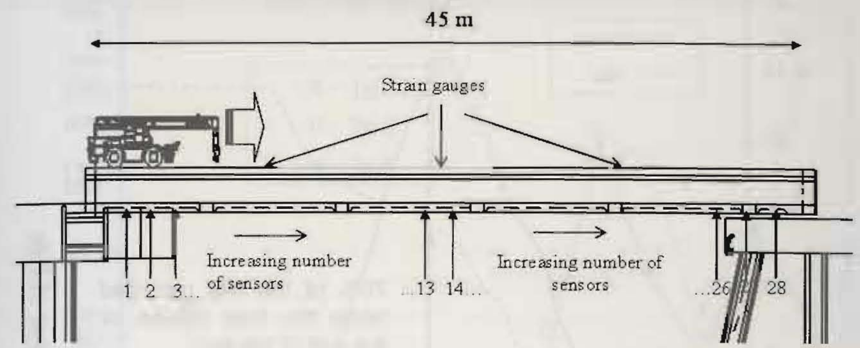

Figure 8.4 Representation of the crane passing over the bridge and sensor location.

The interpretation of AE information is not always easy. This is the reason why different indices have been introduced. Some of them utilize the relative number of hits during the loading and unloading process, or the load at which the AE activity starts compared to the previous maximum load [8.26, 8.27]. Others take advantage of the amplitude distribution of AE events [8.11, 8.20, 8.25, 8.47] and will be discussed later. However, in this case just the total number of AE events during the crane passage sufficed the requirements of the test. The sensor separation of 1.5 m, enabled the recording of most events by at least two adjacent sensors, leading to the calculation of the exact position of the sources in the longitudinal axis of the spam. Figure 8.6 shows the results of linear location for the tree passages of the vehicle. It is obvious that one half of the bridge exhibited much higher activity compared to the other part. This was consistent for all the passages of the crane revealing that the acoustically "active" part was deteriorated, either due to some differential effect of a deteriorative force (the structure was 3 m above sea surface) or

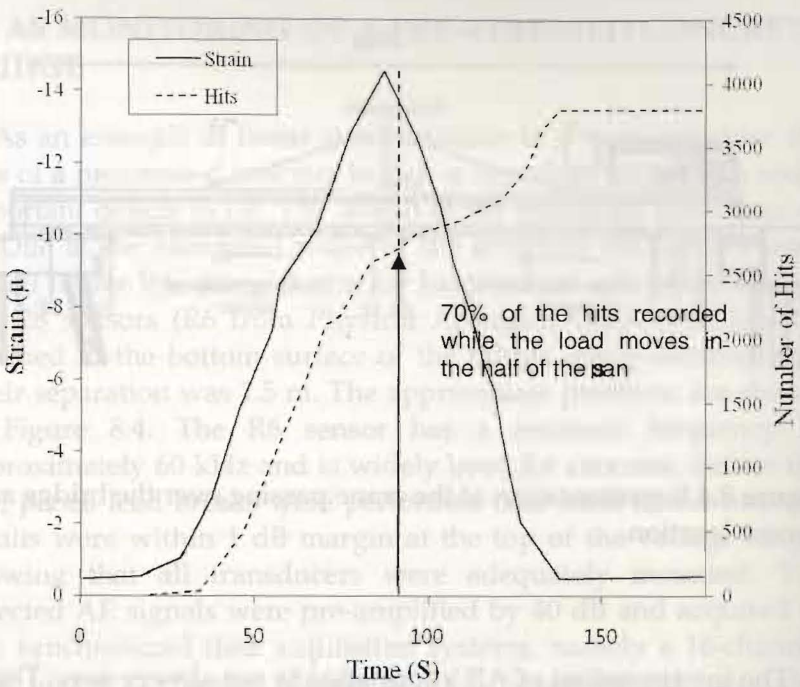

Figure 8.5 Time history of strain at the center and cumulative AE hits during crane passage.

due to inadequate construction. It is well known that the AE activity is connected to the extent of damage through primary (crack growth) and secondary (crack side friction) mechanisms. Therefore, the area which exhibited the highest activity was the most likely to have sustained more serious damage than the rest of the structure examined. Consecutively, this area was selected for the more detailed monitoring using elastic wave velocity which actually revealed a zone of deteriorated material [8.13]. This sequence of procedures reveals that AE can be used as a global monitoring tool in order to scan the whole structure in a fast way, highlight the areas of troublesome integrity of a large structure. Consequently, more detailed examination can be conducted by a pin point method.

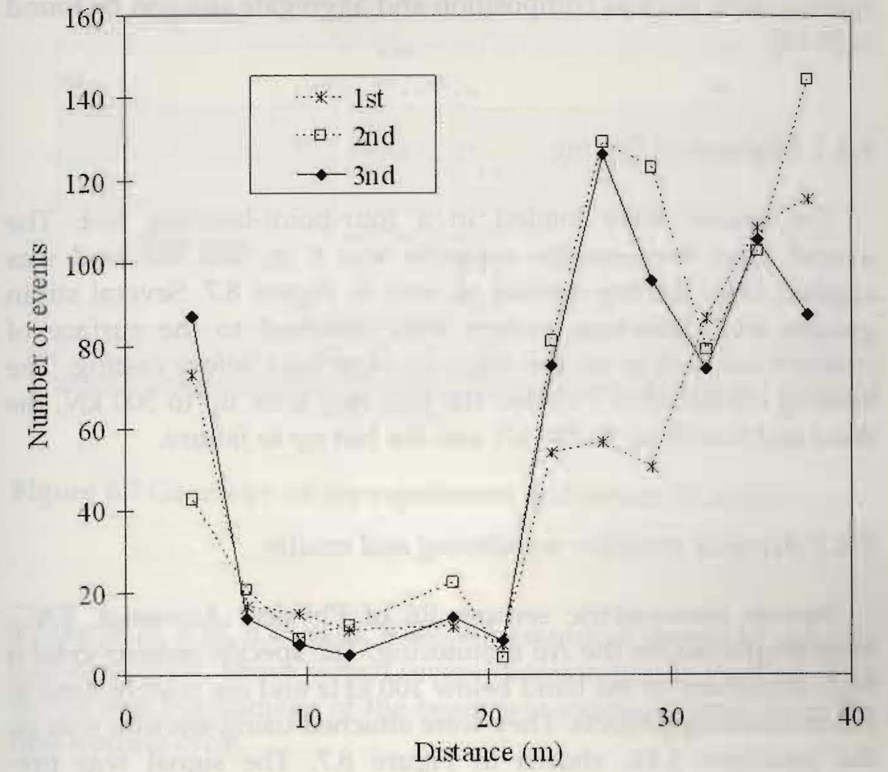

Figure 8.6 Number of events vs. distance from the start of the bridge.

8.4 AE MONITORING DURING BENDING OF LARGE CONCRETE BEAM

Another example comes from the 4-point bending of large concrete beams. The target application of this kind of beams is ground support for tunnel construction. The length was 6.5 m while the cross section was 0.65 m (height) by 1 m. They consisted of two layers of concrete, the lower of which has a thickness of 150 mm. After the complete hydration of this layer (at 28 days) the second layer was cast on top. This layer has large aggregates of 100 mm and quick setting and hardening grout. More details on the construction, such as composition and aggregate size can be found in [8.16].

8.4.1 Mechanical Testing

The beams were loaded in a four-point-bending test. The overall span between the supports was 6 m, and the load was applied from the top surface as seen in Figure 8.7. Several strain gauges and deflection meters were attached to the surface of concrete, as well as on the reinforcement bars before casting. The loading consisted of 5 cycles: the first two were up to 500 kN, the third and fourth up to 750 kN and the last up to failure.

8.4.2 Acoustic emission monitoring and results

Sixteen piezoelectric sensors R6 of Physical Acoustics, PAC, were employed for the AE monitoring. The specific sensors exhibit high sensitivity at the band below 100 kHz and are widely used in AE monitoring projects. They were attached using electron wax on the positions 1-16, shown in Figure 8.7. The signal was pre-amplified by 40 dB, digitized with a sampling rate of 1 MHz and stored in a PAC, DiSP 16 channel system. Apart from the analysis of parameters and waveforms, the AEWin software of PAC provided automatic, real-time event source location during the experiment.

In Figure 8.8 one can see the time history of the cumulative number of AE events along with the applied load. As seen, the AE events are recorded shortly after application of the load. During any cycle of loading and unloading the events increase, finally reaching a number of approximately 8000. This is by itself an indication of intense cracking that happened in the joint beam. What is more important though, is the value of AE indices, like the calm ratio that was mentioned earlier. The activity of the beam was intense even from the first unloading (maximum load of 500 kN). The number of the events during unloading (807) was almost of the same order with loading (1291), leading to a calm ratio of 0.39. This value is related with high degree of damage in relevant

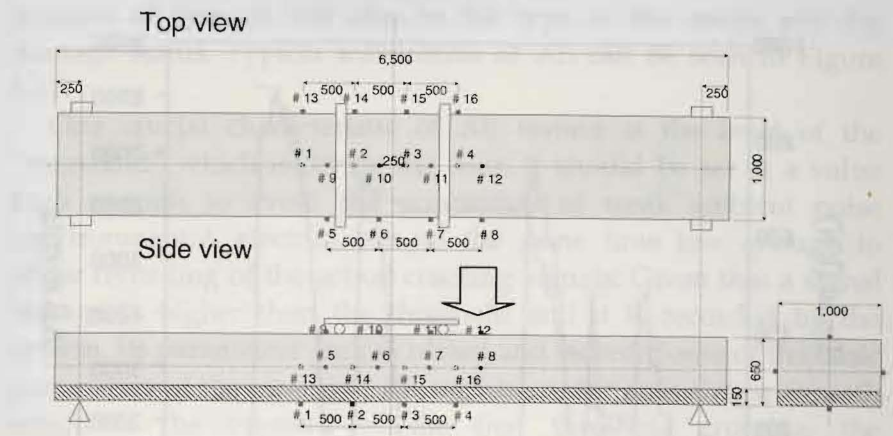

Figure 8.7 Geometry of the experiment and sensor location.

works [8.27, 8.28, 8.45, 8.46, 8.48]. An empirical threshold value of 0.05 is defined, above which severe deterioration is implied. This shows that the damage of the beam was extensive even from the first loading cycle.

8.4.3 Event location

It is interesting to focus on the location of the events. In Figure 8.9 one can observe the location of the events for the first loading and unloading step for the beam. The projection on the different planes (axes x-y and x-z) are presented in different graphs. The events are indicated by circles, the center of which is the location of the source and the diameter stands for the amplitude of the first detected signal of the event. During loading of the 1st cycle there is extensive AE activity, distributed in the whole of the monitored volume. After the maximum load (unloading phase-right graphs of Figure 8.9) the activity is certainly lower, but does not stop, while again the events are located in the whole volume.

It is interesting to discuss the AE activity of the 2nd cycle, which is characterized by the same maximum load as the first (500 kN), as seen in Figure 8.10. The activity is certainly lower, something

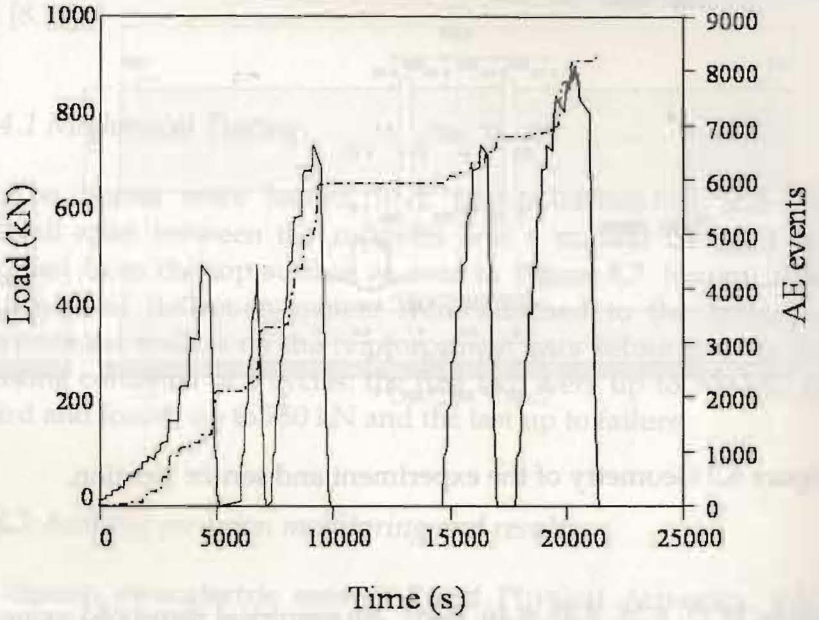

Figure 8.8 AE hits and load history for the joint beam

reasonable due to Kaiser effect; the cracks that may be nucleated or propagate under this load, have already done so in the first cycle. Therefore, only fewer and of lower magnitude events occur. However, even this slight activity for the same load shows that the integrity of the structure has already been compromised. Finally at the last step, which is shown in Figure 8.10b, the activity is again increased, since the maximum load was raised to levels higher than before and new cracks were nucleated or propagated.

8.5 ACOUSTIC EMISSION INDICES

Apart from the deterministic aspects of AE, such as the number of hits and the location of cracks, other qualitative characteristics offer more precise characterization not only on the existence and

location of damage but also on the type of the cracks and the damage status. Typical waveforms of AE can be seen in Figure 8.11.

One crucial characteristic of AE testing is the level of the "threshold" which is set by the user. It should be set at a value high enough to avoid the acquisition of weak ambient noise (environmental, electric) but on the same time low enough to allow recording of the actual cracking signals. Given that a signal voltage is higher than the threshold and it is recorded by the system, its parameters are calculated and stored. Some of the basic parameters of the incoming AE signals are the arrival time (onset), which is the moment of the first threshold crossing, the "Amplitude, A", which is the maximum voltage (either in Volts or dB) exhibited by the highest peak of the waveform, the "Duration" which is the time span between the first and the last threshold crossing. The total number of threshold crossings (which in most cases is equal to the number of waveform peaks) is called "Counts", while the time between the onset and the peak of the highest cycle is called "Rise Time, RT" in μs. The ratio of Amplitude to Rise Time is called Rise Angle or Grade in literature [8.31, 8.49]. Recently the inverse is utilized (RA=Rise Time/Amplitude, μs/V) as suggested by the relevant technical committee [8.1]. The number of Counts divided by the Duration is called "Average Frequency, AF".

In general, the amplitude corresponds to the scale of fracture, since the energy emitted from the source depends on the crack opening displacement; small displacements emit waves of low energy, while large crack propagation incidences generate higher amounts of energy. Characteristics like RT, RA and AF have been correlated to the cracking type (tensile or shear) as will be discussed in more detail later in the chapter. It is generally acceptable that fracture starts from tensile matrix cracking before resulting in shear cracks [8.1, 8.22, 8.40, 8.50]. Therefore, the characterization of the cracking mode can act as a precaution against final failure. The waveform shape depends primarily on the crack type. It can be simply stated that when a tensile event occurs, the sides of the cracks move away from each other, leading to a transient volumetric change in the material and therefore,

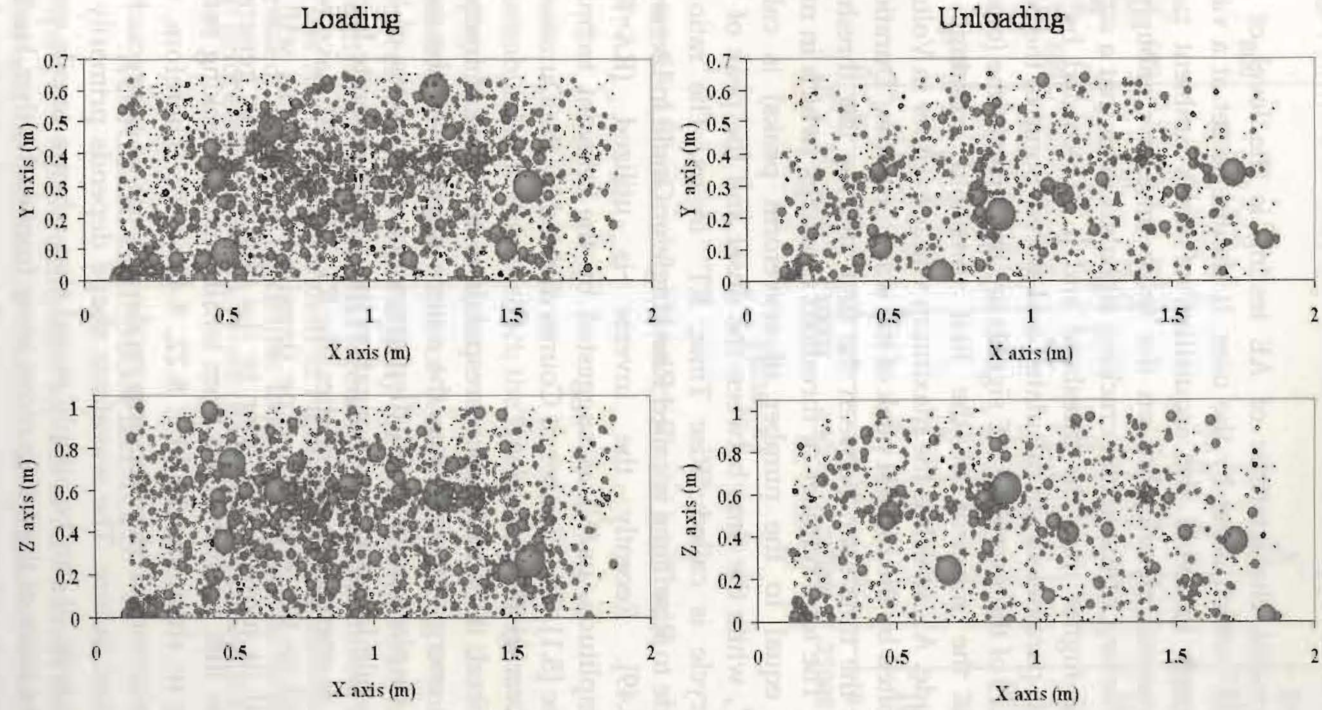

Figure 8.9 Location of AE sources during the first loading cycle.

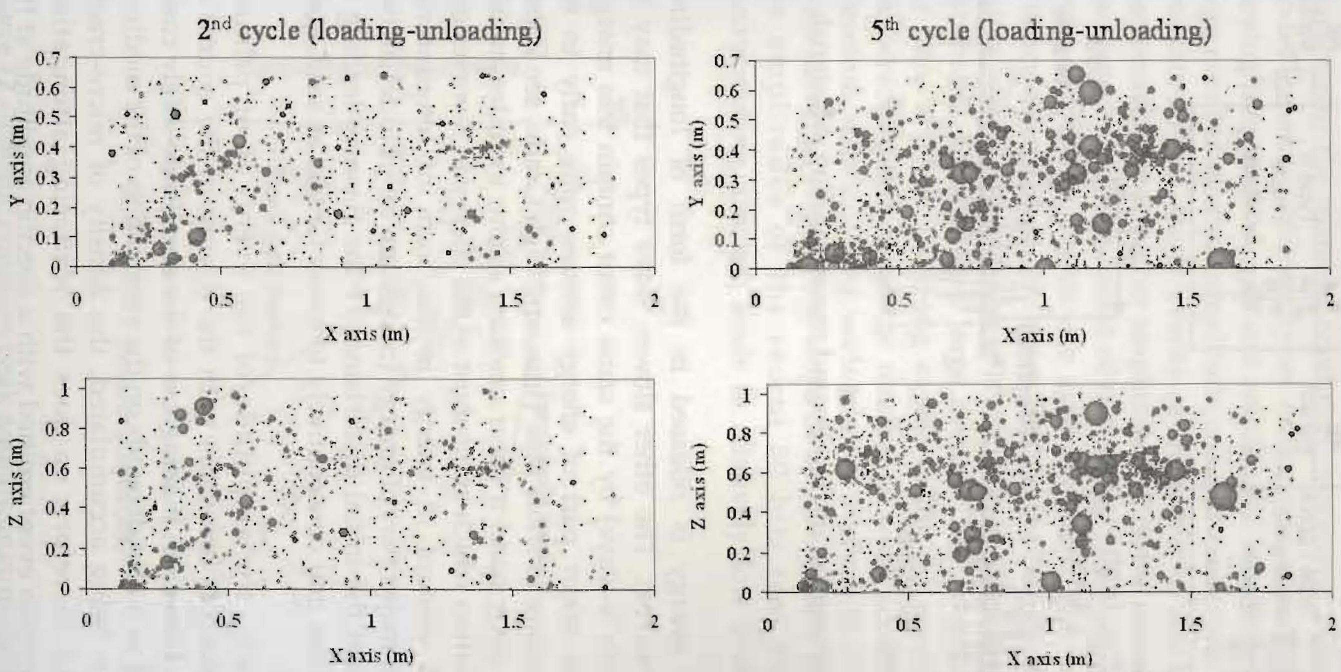

Figure 8.10 Location of AE sources during 2nd and 5th loading cycle.

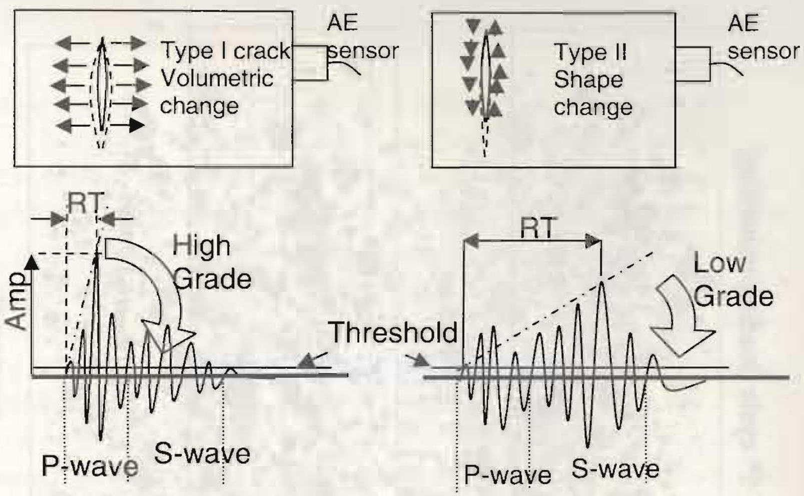

Figure 8.11 Different crack modes and corresponding AE signal.

most of the energy is released in the form of longitudinal (dilatational waves). The other slower wave types that may be emitted (mainly S-wave) by the same event contain less energy. Therefore, the major part of energy arrives quite early in the waveform, leading to short Rise Time, and high Grade, see Figure 8.11. On the other hand a shear cracking event, includes mainly shape deformation which emits most of the energy in S-waves and only a small amount of energy in the form of longitudinal. Therefore, the major part of energy (maximum amplitude) arrives much later than the initial disturbance of the P-wave, leading to longer Rise Time and consecutively to lower Grade, as seen again in Figure 8.11.

Additionally, the amplitude of the events is of primary importance since it correlates with the energy of the source as stated above. However, making use of the amplitude solely could be misleading as it also depends on the attenuation of the medium. As damage is being accumulated, the density of micro-cracks increases and therefore, so does the scattering attenuation. Therefore, a certain event emitted with a specific amplitude at the source will be more attenuated in damaged state than in an earlier

state, making amplitude not a adequate descriptor to solely characterize the material condition. Moreover, different fracture modes generate different types of acoustic emission signals with varying frequency ranges and amplitudes. Microcracks generate a large number of small amplitude acoustic emissions. Macrocracks generate not so many events as microcracks do; however, the macrocracks are of higher amplitude. When the recently generated macrocracks open up, most of the energy is released. Next, many small amplitude events are again created. The occurrence of primary events alters the stress field in the neighbourhood of the source region. Therefore, it is reasonable to affect also the relative distribution of small and large events. The "*Ib*-value" represents the ratio of weak to strong events [8.20]. As mentioned above, microcracks generate a large number of weak acoustic emissions. Therefore, microcracking leads to a relatively high *Ib*-value, which is the absolute value of the slope of the cumulative distribution of the amplitudes of the recent 50 hits (see Figure 8.12). Macrocracking, instead, leads to relatively low b-values since it

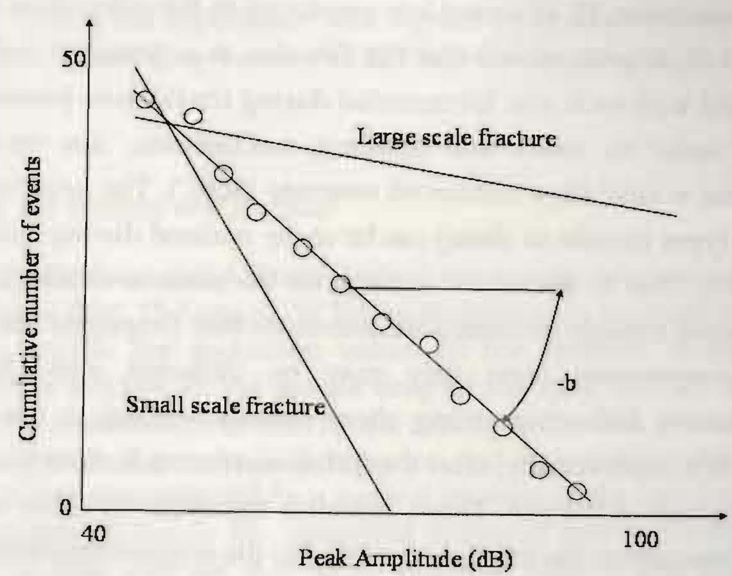

Figure 12 Acoustic emission peak amplitude cumulative distribution.

creates relatively more of the strong events. With increasing stress levels, the fracture process moves from micro- to macro-cracking and the *Ib*-value decreases. Thus, an *Ib*-value decrease can be interpreted as a successive stress accumulation due to a propagating rupture front. For the thorough analysis of *Ib*-value, the interested reader is directed to the original work of Shiotani et al. [8.25]

The formula for the *Ib*-value calculation is defined as:

$$Ib = \frac{\log_{10} N(\mu - \alpha_1 \cdot \sigma) - \log_{10} N(\mu + \alpha_2 \cdot \sigma)}{(\alpha_1 + \alpha_2)\sigma} \tag{8.1}$$

where σ is the standard deviation of the magnitude distribution of one group of recent hits (in our case 50), μ is the mean value of the magnitude distribution of the same group of events, and α_1 and α_2 are constants that define which part of the population will be taken into account. Usually α_1 and α_2 are given the value of 1 and the population, N, of recent hits employed in the calculation is 50 or 100. It is understood that the *Ib*-value is a transient feature, updated with each new hit recorded during the fracture process.

In order to study the different mechanisms, one suitable material is steel fiber reinforced concrete (SFRC). The sequence of crack types (tensile to shear) can be easily realized during bending of SFRC. Due to the tensile stresses on the surface, tensile matrix cracks are initially nucleated. However, as they propagate towards the compression zone they may be deflected and change orientation, following strong shear stresses vertical to the load direction. Additionally, after the initial matrix crack, fiber pull out events start to happen. These, resemble the shear type due to the displacement of the interfaces parallel to the original orientation of the crack. An example of the effect of the failure mode to the AE waveform shape and amplitude distribution can be seen below. The study involved 4-point bending of SFRC specimens.

8.6. ACOUSTIC EMISSION OF STEEL FIBRE REINFORCED CONCRETE

8.6.1 Experimental details

The specimens used in this study were 100x100x400 mm in size. The fibre content was 1% by volume, while the shape of the fibres was wavy with length of 25 mm and diameter of 0.75 mm. The water to cement ratio by mass was 0.5 and the maximum aggregate size was 10 mm. The specimens were tested in four-point bending. The bottom and top spans were 300 mm and 100 mm respectively, as seen in Figure 8.13a. The displacement rate was 0.08 mm/min and the maximum mid span deflection was 2 mm according to ASTM C1609/C 1609M-05. Details on the mechanical testing can be found in [8.51]. Two AE broadband sensors (Pico, PAC) were attached to the bottom tensile side of the specimen (Figure 8.13b). Roller bearing grease was used for acoustic coupling while the sensors were secured by the use of tape during the experiment. The signals were recorded in a two-channel monitoring board PCI-2, PAC with a sampling rate of 5 MHz.

8.6.2 AE activity and Ib-value

Typical Load and AE cumulative hits vs. time curves are shown in Figure 8.14. The rate of AE hits is progressively increasing as the load reaches the maximum value. At the moment of fracture, which is evident by the instant drop of the load, the AE hit rate exhibits a maximum as seen by the almost vertical hit line. In most cases there was a multi-peak behavior, and each of the instant load drops was accompanied by a vertical increase of the hits line. This is reasonable due to the numerous events of matrix cracking, as well as fiber pull out that occur in a time span of less than 1 s. Specifically, more than 100 hits were recorded during each main cracking incidence. After the load drop, the AE rate decreases but the activity does not stop. The typical activity recorded in each test was approximately 1000 hits.

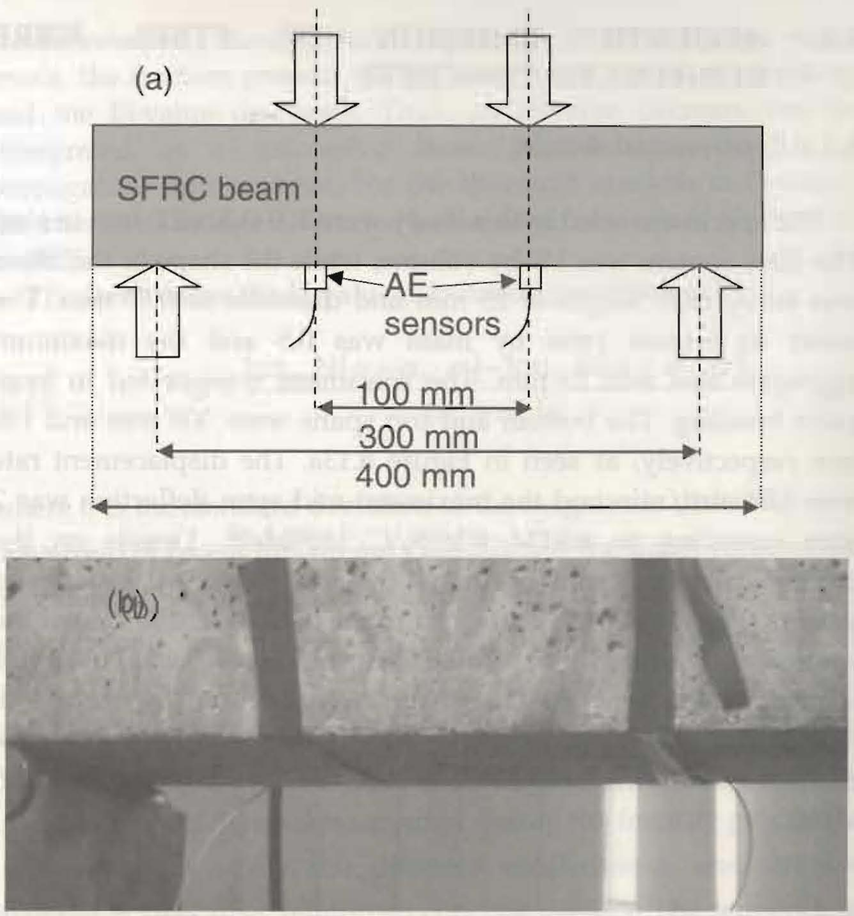

Figure 8.13 (a) Schematic representation of four point bending of concrete with AE monitoring, (b) close up of the AE sensors during experiment.

Figure 8.15 shows the Ib-value history for the same specimens, which as mentioned earlier quantifies the slope of the cumulative amplitude distribution of a recent number of hits (usually 50). For each specific case, a strong drop of the Ib curve is exhibited much earlier than the load drop and is marked by an arrow. In all cases, the Ib-value curve exhibits a strong decrease at least 100 s before the macroscopical load drop, and while the load is approximately

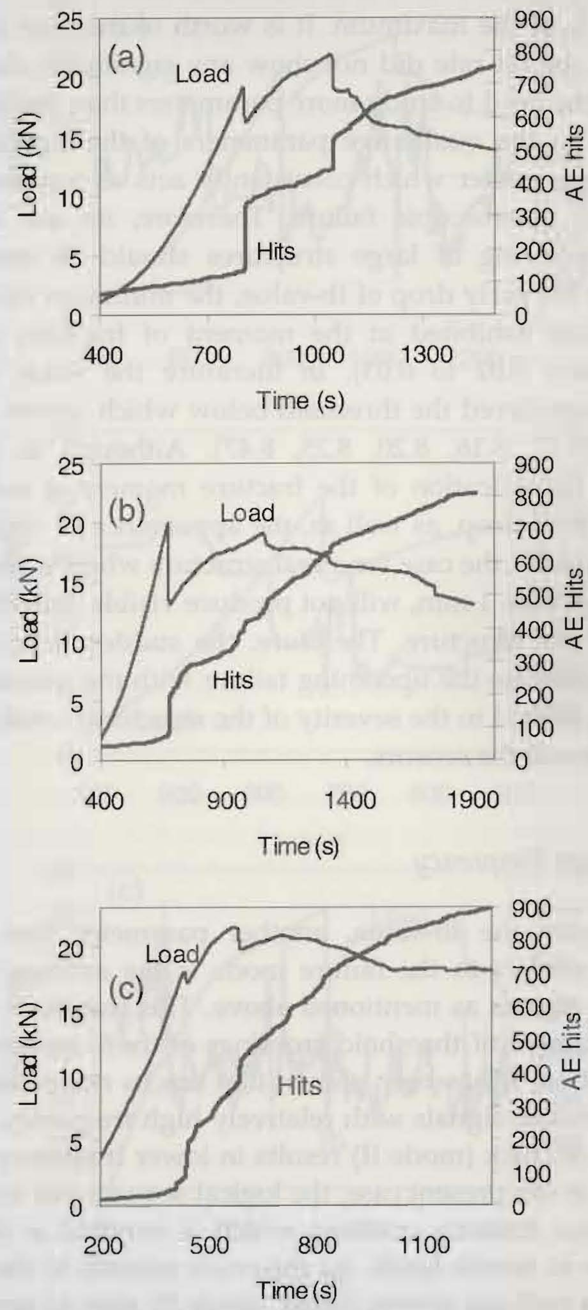

Figure 8.14 Cumulative AE activity and load vs. time for three SFRC specimens.

at 50 to 75% of the maximum. It is worth to mention that at this early time, the hit rate did not show any significant change. This highlights the need to study more parameters than the hit rate and focus also on the qualitative parameters of the signals. The Ib-value is a parameter which consistently acts as a warning much earlier than macroscopic failure. Therefore, its use in case of remote monitoring of large structures should be stressed out. Apart from the early drop of Ib-value, the minimum value of each Ib curve was exhibited at the moment of fracture, (values of approximately 0.02 to 0.03). In literature the value of 0.05 is generally considered the threshold below which severe damage is indicated [8.11, 8.16, 8.20, 8.25, 8.47]. Although in laboratory conditions identification of the fracture moment is not an issue due to the load drop, as well as, the appearance of visible cracks, this is not always the case for a real structure where a similar crack of width less than 1 mm, will not produce visible deflection due to the size of the structure. Therefore, the sudden drop of the Ib-value will indicate the upcoming failure with the minimum value itself being related to the severity of the structural condition of the material around the sensors.

8.6.3 Average Frequency

Apart from the Ib-value, another parameter that has been studied in respect to the failure mode is the average frequency (AF) of the signals as mentioned above. This feature is calculated from the number of threshold crossings of the waveform divided by its duration. It has been shown that cracks resembling mode I (tensile) produce signals with relatively high frequency, while the shear type of crack (mode II) results in lower frequency [8.1, 8.22, 8.40, 8.50]. In the present case, the logical sequence of events starts with the type I matrix cracking which is initiated at the bottom surface due to tensile loads. As the crack extends to the top, fibre friction and pull out events (shear, mode II) start to occur. At the last stage when most of the specimen's cross section has been ruptured and the two parts of the specimen get more separated, the fibre pull out events dominate the process.

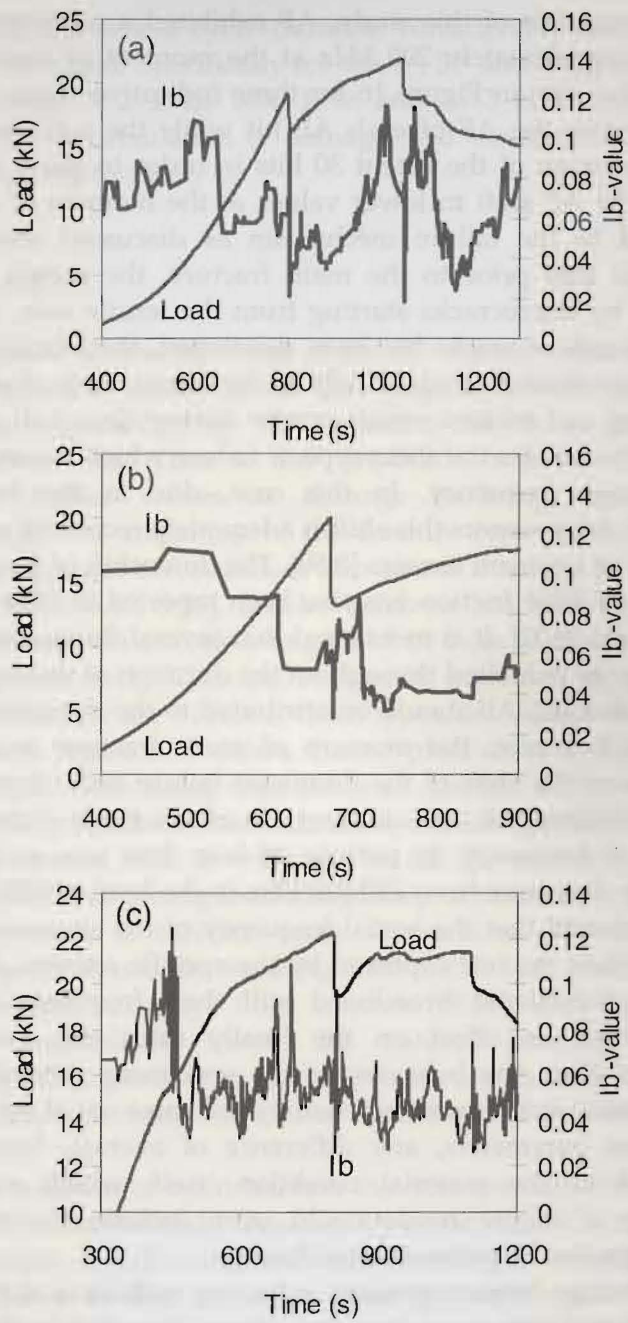

Figure 8.15Ib-value and load vs. time for three SFRC specimens

For the materials of this study, AF exhibited a consistent strong drop of approximately 200 kHz at the moment of main failure. This can be seen in Figure 16 for three indicative cases. The dots correspond to the AF of each AE hit while the solid line is the moving average of the recent 30 hits in order to show the trend clearly. The AF shift to lower values at the moment of failure is connected to the failure mechanism as discussed above. It is reasonable that prior to the main fracture, the matrix is being ruptured by microcracks starting from the tensile side. After the main network of cracks has been developed, the tensile cracking events give their place gradually to the shear mode due to fibre debonding and friction which occurs during fibre pull out. This behavior resembles the shear type of failure which is connected to low average frequency. In this case, due to the broadband response of the sensors this shift is adequately recorded, compared to the use of resonant sensors [8.50]. The downshift of frequency at the stage of fibre friction has also been reported in fibre pull out experiments [8.22]. It is mentioned that several fluctuations of the curve may be exhibited throughout the duration of the experiment (see Figure 8.16). All should be attributed to the dynamic fracture behavior; however, the moment of main fracture is the most indicative of the shift of the dominant failure mode from matrix cracking to fibre pull out and results in severe drops of the moving average of frequency in periods of less than one second. The frequency decreases from 250-320 kHz to the level of 100-150 kHz. It is mentioned that the actual frequency of the sources could be different than the one captured by the specific sensors. Although they are considered broadband still their frequency response should have an effect on the finally calculated parameters. However, since the behavior of the specimens throughout the experimental series were recorded by the same set of sensors and acquisition parameters, any difference of average frequency is connected to the material condition itself, which except the changing of failure mode could even include the increasing attenuation due to accumulating damage.

The average frequency seems to be very indicative of the failure mode in small specimens but proved sensitive also for the case of the large beam which was tested in 5 cycles bending and was discussed in section 4. The AF measured from all the sensors

throughout the whole cycle duration considerably decreased as the load increased. Specifically for the 1st, 3rd and 5th cycle, the AF values where 60.2 kHz, 55.6 kHz and 49.2 kHz respectively, showing the accumulation of damage, and the shift from tensile matrix cracking to shear.

8.6.4 RA value

As mentioned above, the shape of the AE waveforms is related to damage type and accumulation. The shape of the first part of the waveform is quantified by "RA" which is defined as the ratio of the waveform Rise Time to the Amplitude in μs/V. This value shifts to higher values as damage is being accumulated. Additionally, the transition of the fracture type from the initial tensile to the shear before failure also causes this kind of RA value shift [8.1, 8.11, 8.40, 8.50]. Similar behavior has been reported in laminated composites concerning the shift from matrix cracking to delaminations [8.41]. This can be simply explained by the wave modes excited by the different crack types, as discussed earlier in the chapter. Figure 8.17 shows three typical cases of RA moving average with time along with the load history. Before the main fracture event which is demonstrated by the sudden load drop, RA averages around 500 to 1000 μs/V. At the moment of main fracture it exhibits strong local maxima up to more than 4000 μs/V and afterwards it exhibits some fluctuations on a generally increasing trend, usually reaching 2000 μs/V. This trend has also been observed on vinyl fibre concrete [8.11], and shows that different mechanisms inside the material produce different signature AE signals. The initial events are caused by matrix cracking and therefore, due to their tensile nature they exhibit low RA.

At the moment of main fracture the mid span deflection of the specimen instantaneously increases by some tens of a mm and a great number of pull-out events occur, leading to a sharp peak of the RA curve at that moment. After the main crack has been formed the pull-out events obtain a more controlled rate due to the constant displacement rate, leading eventually to higher RA values than before main fracture.

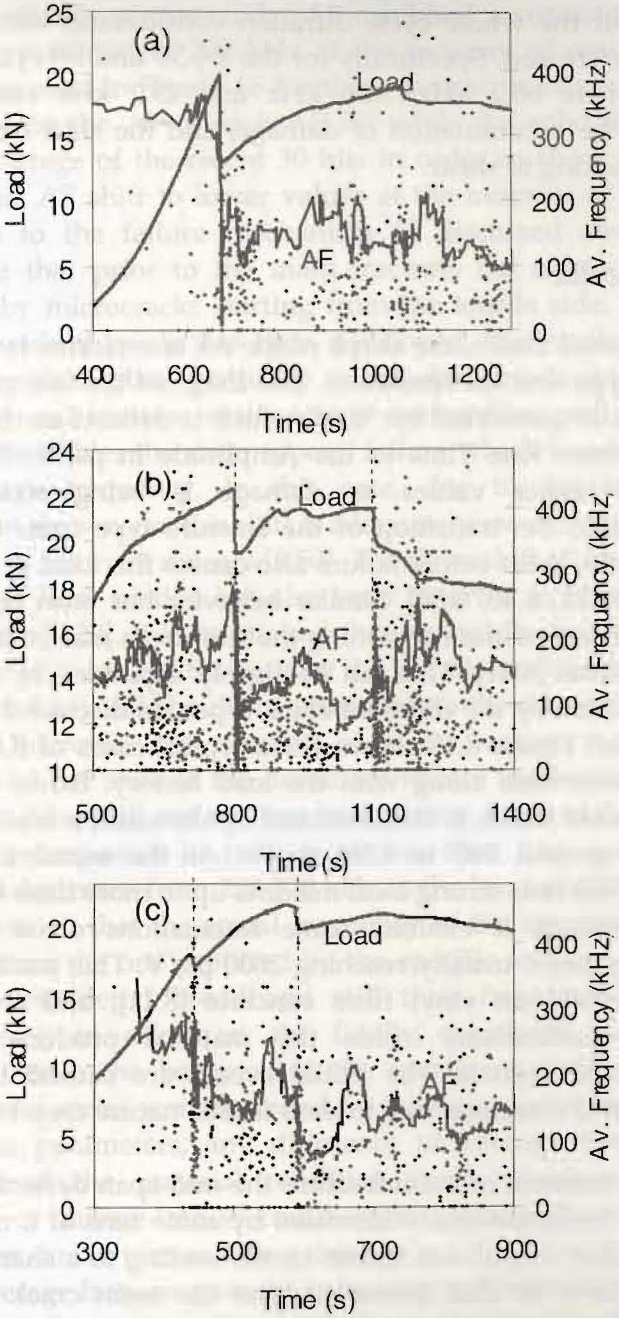

Figure 8.16 Average frequency and load vs. time for three SFRC specimens.

It is seen that AE parameters, which quantify the shape of the waveforms follow the fracture process closely. This is evident especially at the moment of main crack formation before which only tensile matrix cracking occurs while after, the main mechanism is fiber pull out. This shift of failure mechanisms is primarily reflected on the average frequency of the signals, which is instantly reduced by hundreds of kHz, and secondarily on the RA value, which exhibits strong local maxima at those moments, while it retains an increasing trend throughout the duration of the experiment. These strong discrepancies throughout the failure process confirm that SFRC is an adequate model material to study the correlation between AE behavior and the different fracture mechanisms. Additionally, they build an understanding on the sequence of the fracture mechanisms and their fingerprint on AE signals, which can be used for actual monitoring of concrete structures.

8.6.5. Effect of propagation distance

The above measurements are quite consistent in laboratory conditions, for a specific specimen size and loading pattern. Therefore, they are useful to evaluate which are the most sensitive parameters of the AE signals to the materials integrity. As mentioned above, the ultimate goal of AE is to be implemented in situ and estimate the condition of the material. In order to do so, it would be desirable that specific values of these indices should be established characterizing the different conditions of the material (healthy-questionable-poor). Although this would be easy in laboratory conditions, the situation at a real structure employs many more random parameters. One is the distance between the source crack and the receiving transducers. Due to logistics and time restrictions in actual AE monitoring cases, the sensors distance is usually longer than 1 m. This means that most of thesignals will travel distances of the order of 1 m or more until they are recorded by one or more adjacent sensors. In case the material behaves in a completely homogeneous way, the waveform shape and the corresponding parameters will not change in 3-dimensional bulk propagation. However, since the AE

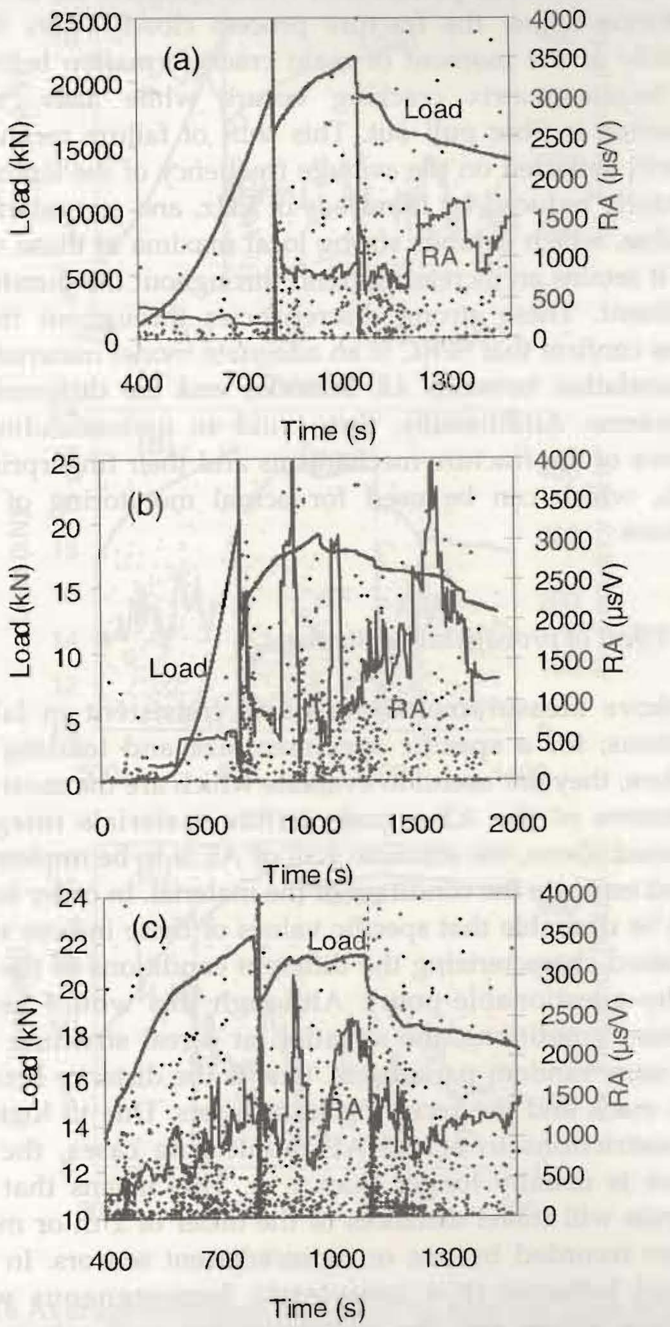

Figure 8.17 RA and load vs. time for three SFRC specimens.

sensors are attached on the surface, Rayleigh waves will also be included in the received waveform, since part of the energy will be converted from P- and S- wave to Rayleigh when the wave meets the surface. Due to the different velocity of the distinct modes the waveform will constantly change shape, as the shear and Rayleigh waves will progressively delay more after the initial P-wave. Furthermore, in concrete which is inhomogeneous by nature, including sand and aggregate grains, as well as air voids and cracks, the shape of a propagating pulse will be distorted due to scattering. This is called "dispersion" which is a phenomenon that dictates that different wavelengths propagate with different velocity [8.5, 8.6, 8.52, 8.53]. Since the original pulse consists of different frequency components it is reasonable that the shape of the pulse is distorted and its duration increased. Therefore, any parameter calculated on a signal at a specific distance will likely differ from the same signal after propagation to a further sensor.

8.6.6. Numerical simulation

In order to study the effect of propagation distance in an inhomogeneous material like concrete, numerical simulations were conducted as explained in the following.

The fundamental equation governing the two-dimensional propagation of stress waves in a perfectly elastic medium, ignoring viscous losses is as follows:

$$\rho \frac{\partial^2 u}{\partial t^2} = \mu \nabla^2 u + (\lambda + \mu) \nabla \nabla \cdot u \qquad (8.2)$$

where u=u(x,y,t) is the time-varying displacement vector, ρ is the mass density, λ and μ are the first and second Lame constants respectively, and t is time. In simulation, certain prerequisites should be followed in order for the analysis to lead to reliable results. The simulations were conducted with commercially available software [8.54]. It operates by solving the above equation based on the method of finite differences. Equation (8.1) is solved with respect to the boundary conditions of the model, which include the input source that has pre-defined time-dependent displacements at a given location and a set of initial conditions [8.55]. For heterogeneous media wave propagation in each distinct homogeneous phase (in this case mortar matrix and inclusions) is solved according to Eq. (8.1), while the continuity conditions for stresses and strains must be satisfied on the interfaces [8.55].

The materials were considered elastic with damping. The numerical model included the mortar matrix, round aggregates and in some cases cracks, simulated by thin rectangles of 20x2 mm. The corresponding properties of the materials used in the model can be seen in Table 1. Aggregates were assumed slightly stiffer than the matrix, while damping parameters were also included guided by relevant experiments [8.56]. The material used for the cracks was assigned properties of air, see again Table 1.

The spacing resolution was set to 3 mm which is less than one tenth of the excited wavelength (approximately 47 mm), while the sampling time was 0.193 μs, much less than the period of the excited wave (10 μs), enabling each cycle to be represented by approximately 50 points, while 20 points are considered satisfactory in similar simulations [8.57]. The geometry of the model is seen in Figure 8.18. It represents a 2 m long concrete beam with a width of 0.4 m. Apart from the case of

Table 8.1 Properties of materials used in the numerical model

	λ GPa	μ GPa	ρ kg/m³	C_P m/s
Mortar Matrix	11.1	16.6	2300	4735
Aggregates	14.3	25.4	2600	5190
Cracks	10^{-4}	10^{-6}	1.2	300

inhomogeneous but intact concrete which was simulated initially, different cases of crack density were examined. Specifically, the cases concerned cracks at percentages of 1.4%, 2.8% and 5.7% of the whole cross section of the specimen. The "receivers" were placed on the top surface of the geometry, with a separation distance of 300 mm and provided the average vertical displacement over their length, meaning that each receiver's signal represents the average response over a number of nodes. The snapshots of Figure 8.18 show the wave spreading away from the point source at three distinct moments after excitation. The excitation was one cycle of 100 kHz. It is worth to mention that due to the strong scattering that the inhomogeneity of concrete imposes, the S-wave is not easy to be recognized.

As the wave front spreads it reaches the adjacent transducers and the transient response of the sensors is recorded. Typical waveforms of 4 receivers are seen in Figure 8.19.

It is evident that apart from the delay imposed to the waveform of the following transducers, there is also a strong influence on the

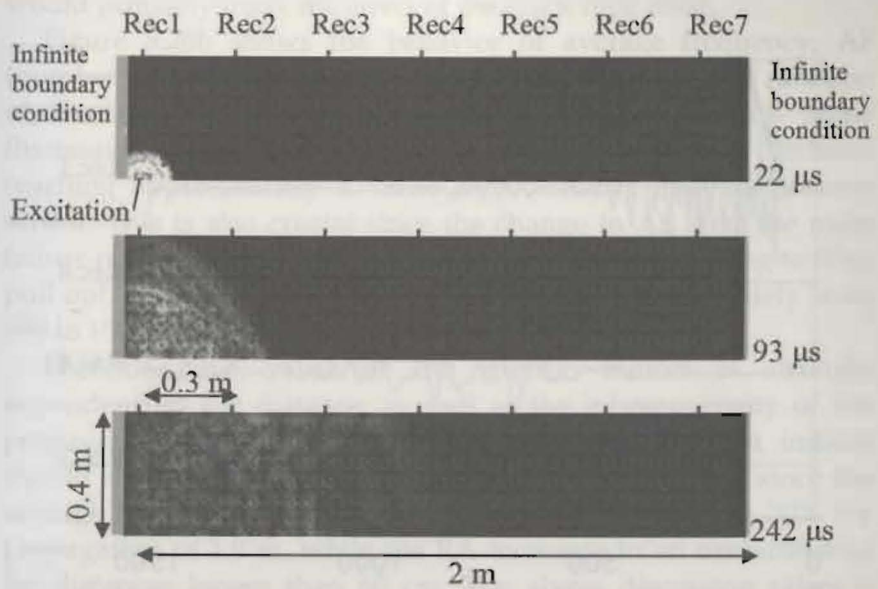

Figure 8.18 Geometric model and consecutive snapshots of the displacement field.

shape of the pulse. Specifically, Receiver 1 which is placed vertical from the excitation records a signal with high grade, which reaches its maximum shortly after the onset. However, as the distance increases, the grade of the waveform decreases and the maximum amplitude delays more, relatively to the onset, as seen for Receiver #7 in Figure 8.19. By calculating the specific waveform parameters that are of interest for AE one can draw valuable conclusions for their dependence on propagation distance.

Figure 8.20a shows the RA values calculated for the different receivers, as a function of the horizontal distance from the source and the different material conditions. It can be seen that for the case of plain concrete, the RA stays approximately constant up to the distance of 1.5 m, but becomes unstable at 1.8 m. This change in the RA of the pulse, is evident at closer distance if the material contains cracks, something reasonable due to the increased scattering dispersion. For the case of cracks at a percentage of roughly 6%, the RA becomes unstable at distances longer than 0.6 m. Therefore, it can be concluded that both propagation distance

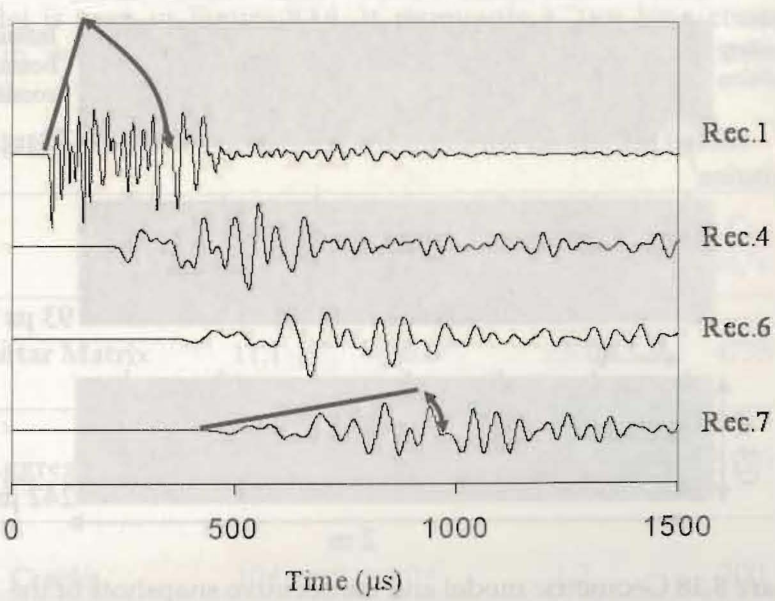

Figure 8.19 Simulated waveforms collected at different sensors

and material condition strongly influence the shape of the pulse. The rise angle and other waveform parameters although depend on the mode of the crack, can be severely influenced by propagation through damaged material. This practically means that a specific tensile event recorded by a close transducer in intact concrete will be characterized as mode I, while if the material is deteriorated and the receiver is placed away from the source, it would more likely be characterized as mode II. This dependence of RA on material and testing parameters is crucial. The distance in combination to the material's condition may lead to an increase of the RA by 30 to 200 times, meaning that this change would more likely mask the actual source, falsely shifting the characterization in favor of the mode II. It is reminded that the actual change of RA based on the cracking type alone as was measured experimentally for SFRC, and described earlier in the text, was of the order of 4-10. Specifically, the RA before the main cracking was less than 500 μs/V, while later it increased to about 2000 μs/V. Even at the moment of fracture the local maximum reached approximately 4000 μs/V, increasing by a factor less than 10 (see again Figure 8.17). Therefore, a change by 30 or more times due to distance would probably mask the effect of the crack type itself.

Figure 8.20b shows the behavior of average frequency, AF (number of threshold crossings over signal duration) as a function of distance for different material conditions. Despite some fluctuations there is a decreasing trend of AF with distance reaching approximately a value 20-30% lower than the nearest sensor. This is also crucial since the change in AF after the main failure of the specimens, and the shift from matrix cracking to fiber pull out, was also of the same order (50%, i.e. approximately from 300 to 150 kHz, as exhibited in Figure 8.16).

Therefore, the value of the specific indices is strongly dependent on the distance, as well as the inhomogeneity of the propagation path. The specific values of the different indices should always be connected to the propagation distance, since the average frequency may suffer a decrease of as much as 30% for propagation of 1.8 m, while the RA increases in an unstable way for distances longer than 60 cm. The above discussion raises a crucial subject concerning AE monitoring of large structures. It shows that in order to characterize the cracking mode, data should

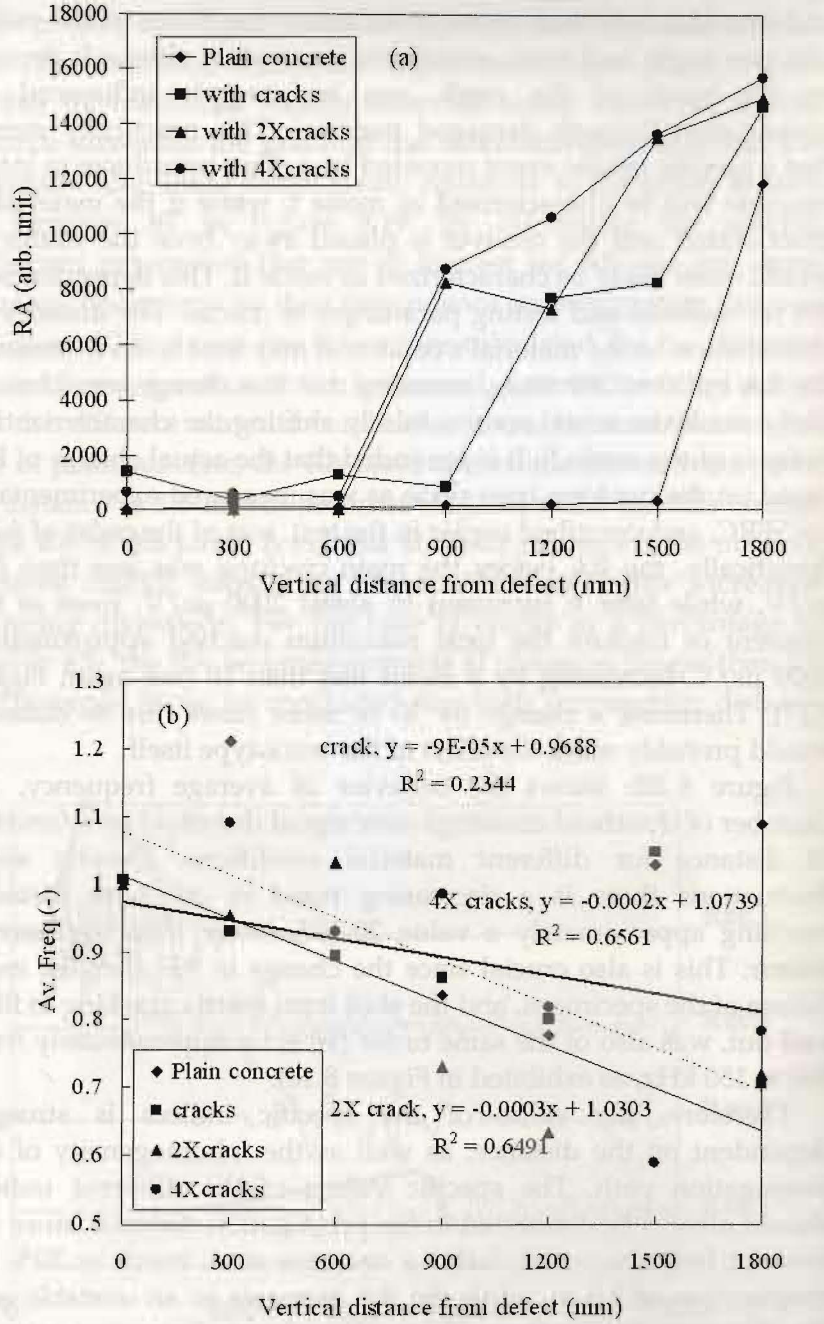

Figure 8.20 Simulated results of (a) RA and (b) average frequency vs. horizontal distance between source and receiver.

be collected by sensors at close distances. In case the separation distance of the receivers is longer than a threshold value (60 cm, as suggested by the above simulations) the data should not be treated as a group but should probably be categorized according to their distance from the source in order to be used for cracking mode characterization. Apparently, the above discussion does not include the deterministic aspects of AE, like event location, which are not influenced by the shape of the waveform, but only from the arrival time of the signal. In practical terms, location of the cracking zones may be conducted even for long distance between the AE sensors, but when detailed assessment of the failure mode is attempted, the receivers should be quite close, or take into account the events located very close to the receivers. The above considerations after proper study will hopefully enhance the characterization for in-situ applications.

8.7 EXAMPLE OF IN-SITU MONITORING BASED ON AE INDICES

As an example of characterization of materials concerning the damage type, the AE monitoring of rock is described. Rock failure and landslides are some of the frequent disasters [8.31]. The rock material is of brittle nature and therefore, micro- and macro-fracture progresses as a transient phenomenon. It may start with slight movement between the joints of the rock masses. The signals emitted by the dislocations may be evaluated in order to predict the slope failure. Due to the inherent attenuation of the materials, low frequency sensors should be employed. Moreover, AE waves generated within the rock are certainly reflected by the joints within the material, and therefore, the sensors are placed in a waveguide which greatly enhances wave propagation [8.32]. The waveguide is a tube including a steel bar which effectively acts as the wave carrier, on which the sensors are attached. The rest is filled with cementitious material. In this case, the moving mass of rock will cause fracture of the tube and the cementitious material within [8.31]. Therefore, AE waves are generated by the fracture of the filler itself (Figure 8.21). The properties of the filler are defined by tests on the actual rock material after borehole excavation. Similar specimens are prepared and tested in four-point bending in order to monitor the AE due to their fracture in laboratory. The fracture of the waveguide-filler specimen is similar to this of the deformed rock. As a result, the characteristics of the AE waves, generated within the waveguide would be compatible to the actual rock deformation. Therefore, comparing field data with the laboratory data obtained for bending experiments, the fracture state of the rock can be readily available.

Results from laboratory tests concerning the "Grade" of AE hits, are shown in Figure 8.22 [8.32]. It is shown that grade experienced an almost constant decrease throughout the bending load increase. Failure starts by vertical tensile cracks but later it is deflected to other orientations, due to strong shearing, decreasing the grade of the AE waveforms.

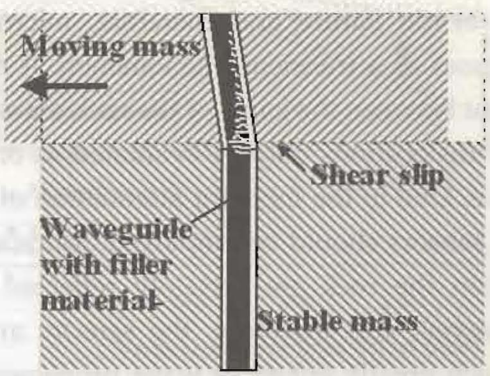

Figure 8.21 Representation of rock dislocation with waveguide.

From this test it can be concluded that Grade values above 5 are related to low damage level, while tensile fracture is still dominant. However, later Grade reduces indicating the final stage of fracture, as well as the shift of the cracks from tensile to shear.
After installation of the sensors in the borehole of inside the rock, monitoring commenced and was continued for long periods of time while the results were recorded. Different parameters were continuously analyzed. The time history of the Grade monitoredby 3 sensors is indicatively shown in Figure 8.23.

It is seen that for most of the monitoring period, grade lies above 10, which shows relatively low stress on the waveguide and therefore, low rate of movement on the rock. However, on a specific date (around 12/1) there was a strong and abrupt decrease in the grade of the acquired signals. Especially sensor #3 recorded a grade of 5, which implies the generation of shear fracture around the location of sensor 3.

The AE hit rate is also depicted along with the strain rate which was monitored inside an adjacent borehole (Figure 8.24).

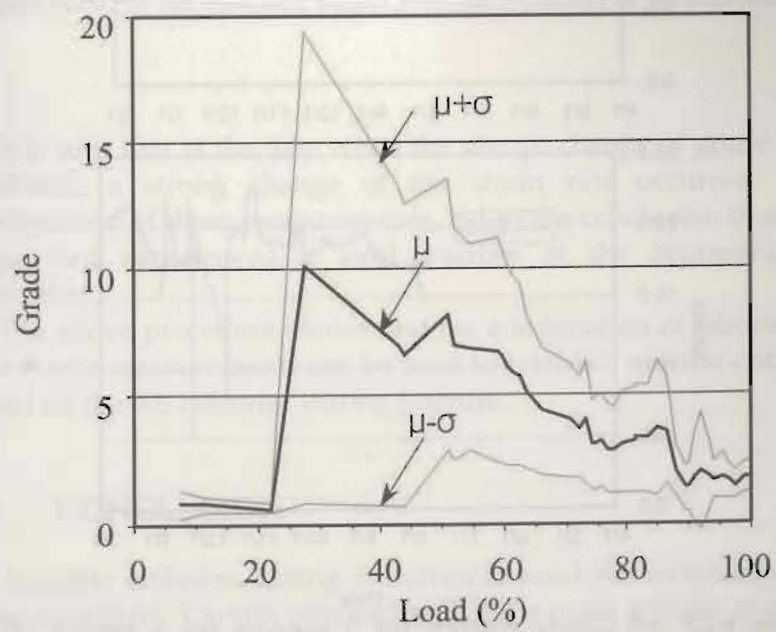

Figure 8.22 Variation of AE grade according to the applied load

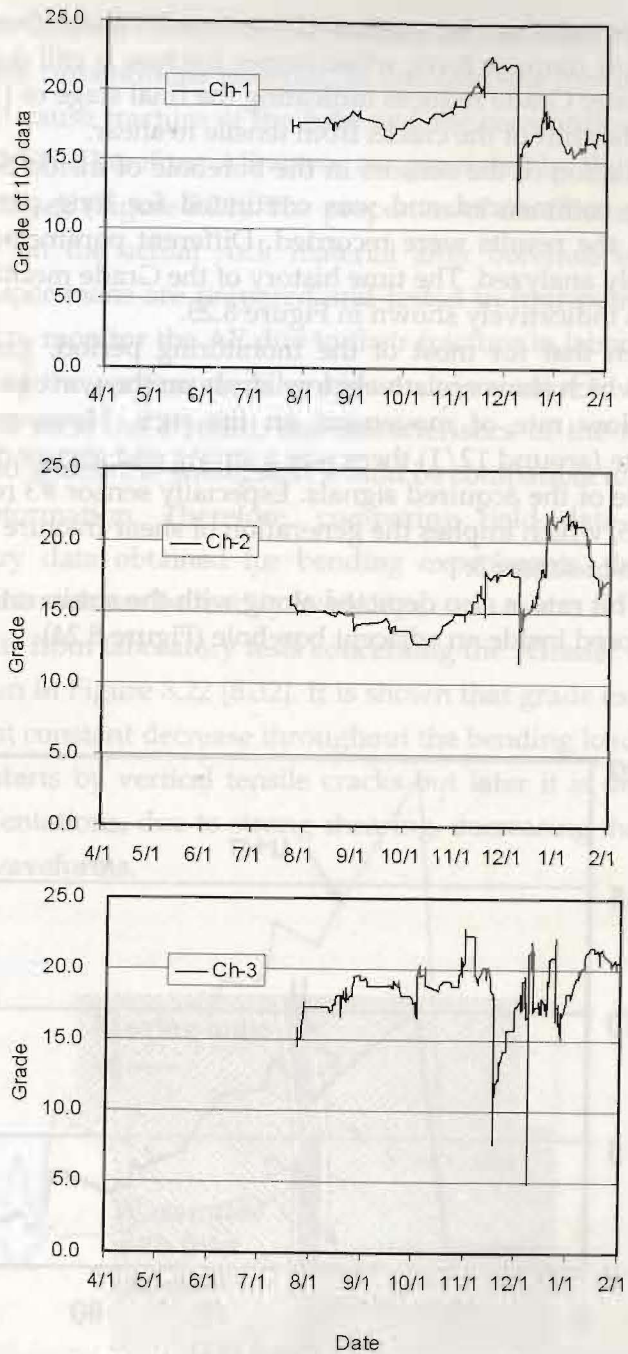

Figure 8.23 AE Grade history for 3 sensors for a period of 10 months.

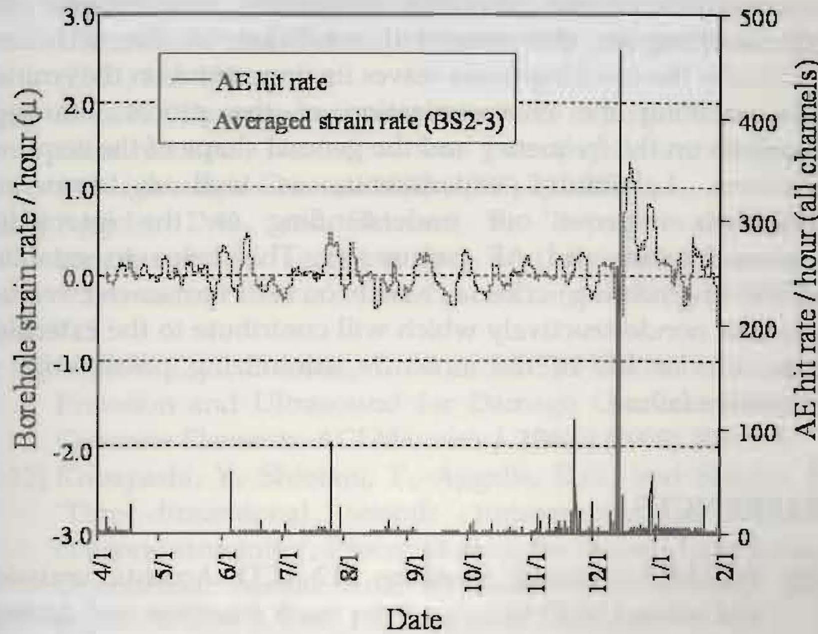

Figure 8.24 AE hit rate and strain rate for a period of 10 months.

It is seen that at the date when the abrupt change of grade was exhibited, a strong change of the strain rate occurred. The combination of these measurements, led to the conclusion that the slope had experienced a local fracture at the beginning of December.

The above procedure shows that the combination of laboratory and in-situ measurements can be used to establish specific criteria, based on the AE behavior during fracture.

8.8 CONCLUSION

Acoustic emission testing is currently used for monitoring of large structures. Certain parameters like the crack activity and the location of the failure zones are the kind of critical information usually offered by the test. More detailed analysis of the characteristics of the acquired waveforms can enhance the understanding on the structural condition of the structure. Specifically the cracking mode leaves its fingerprint on the emitted wave enabling the characterization of the process, through alterations on the frequency and the general shape of the acquired waveform. Laboratory experiments, as well as numerical simulations improve our understanding on the interaction between fracture and AE parameters. This helps to establish specific engineering criteria based on AE parameter values measured nondestructively which will contribute to the extension of the service life of the structure minimizing possibilities of destructive failure.

REFERENCES

[8.1] RILEM Techincal Committee 212-ACD. Acoustic emission and related NDE techniques for crack detection and damage evaluation in concrete (2004-2009).

[8.2] RILEM Techincal Committee MCM: On-site measurement of concrete and masonry structures by visualized NDT, 2010-(active).

[8.3] Naik, T. R., Malhotra, V. M. and Popovics, J. S., 'The Ultrasonic Pulse Velocity Method', in 'CRC Handbook of Nondestructive Testing of Concrete', Eds Malhotra V.M., Carino N. J., CRC, Boca Raton, FL, 2004.

[8.4] Shiotani, T., Momoki, S., Chai, H.K. and Aggelis, D. G., 'Elastic wave validation of large concrete structures repaired by means of cement grouting', *Constr. Build. Mater.*, **23**(7) (2009) 2647-2652.

[8.5] Aggelis, D. G. and Philippidis, T. P., 'Ultrasonic wave dispersion and attenuation in fresh mortar', *NDT & E International* **37**(8) (2004) 617-631.

[8.6] Philippidis, T.P. and Aggelis, D.G., 'Experimental study of wave dispersion and attenuation in concrete', *Ultrasonics* **43**(7) (2005) 584-595.

[8.7] Kaplan, M.F., 'The effects of age and water/cement ratio upon the relation between ultrasonic pulse velocity and compressive strength', *Mag. Con. Res.* **11**(32) (1959) 85-92.

[8.8] Popovics, S., 'Analysis of the Concrete Strength versus Ultrasonic Pulse Velocity Relationship', *Mater. Eval.* **59**(2) (2001) 123-130.

[8.9] Ono, K., 'Damaged concrete structures in Japan due to alkali silica reaction', *The International Journal of Cement Composites and Lightweight Concrete* **10**(4) (1988) 247-257.

[8.10] Aggelis, D.G., and Shiotani, T., 'Repair evaluation of concrete cracks using surface and through-transmission wave measurements', *Cem. Concr. Compos.*, **29**(9) (2007) 700-711.

[8.11] Aggelis, D.G., Shiotani, T., Momoki, S., Hirama, A., Acoustic Emission and Ultrasound for Damage Characterization of Concrete Elements. *ACI Materials J.* **106**(6) (2009) 509-514.

[8.12] Kobayashi, Y., Shiotani, T., Aggelis, D.G., and Shiojiri, H., 'Three-dimensional seismic tomography for existing concrete structures', Proceedings of the Second International Operational Modal Analysis Conference, IOMAC 2007, (April 30-May 2, 2007, Copenhagen) **2** 595-600.

[8.13] Shiotani,T., Aggelis D.G. and Makishima O., 'Global monitoring of large concrete structures using acoustic emission and ultrasonic techniques: case study', *J. Bridge Eng.-ASCE*, **14**(3) (2009) 188-192.

[8.14] Chai, H.K., Aggelis, D.G., Momoki, S., Kobayashi, Y., Shiotani, T., 'Single-side access tomography for evaluating interior defect of concrete', *Constr. Build. Mater.*, in print, 2010.

[8.15] Grosse, C.U., Ohtsu, M., 'Acoustic Emission Testing', (Springer, Heidelberg, 2008)

[8.16] Aggelis, D.G. Shiotani, T., and Terazawa, M. 'Assessment of construction joint effect in full scale concrete beams by acoustic emission activity, *J. Eng. Mech.-ASCE*, in print, 2010.

[8.17] Schechinger, B., and Vogel, T., 'Acoustic emission for monitoring a reinforced concrete beam subject to four-point-bending', *Constr. Build. Mater.* **21**(3) (2007) 483-490.

[8.18] Wu, K., Chen, B., and Yao, W., 'Study on the AE characteristics of fracture process of mortar, concrete and steel-fiber-reinforced concrete beams', *Cem. Concr. Res.*, **30** (2000) 1495-1500.

[8.19] Chen, B., and Liu, J, 'Experimental study on AE characteristics of three-point-bending concrete beams', *Cem. Concr. Res.* **34** (2004) 391-397.

[8.20] Kurz, J.H., Finck, F., Grosse, C.U., and Reinhardt, H.W., 'Stress drop and stress redistribution in concrete quantified over time by the b-value analysis', *Structural Health Monitoring* **5** (2006) 69-81.

[8.21] Grosse, C., Reinhardt, H., and Dahm, T., 'Localization and classification of fracture types in concrete with quantitative acoustic emission measurement techniques', *NDT&E Int*, **30**(4) (1997) 223–230.

[8.22] Reinhardt H.W., Grosse C.U., and Weiler B., 'Material characterization of steel fibre reinforced concrete using neutron CT, ultrasound and quantitative acoustic emission techniques', *NDT.net* **6**(5) (2001) (http://www.ndt.net/article/v06n05/ grosse/grosse.htmT)

[8.23] Grosse, C.U., and Finck, F., 'Quantitative evaluation of fracture processes in concrete using signal-based acoustic emission techniques'. *Cem. Concr. Compos.* **28**(4) (2006) 330-336.

[8.24] Shiotani, T., Bisschop, J., and Van Mier J. G. M., 'Temporal and spatial development of drying shrinkage cracking in cement-based materials', *Eng. Fract. Mech.*, **70**(12) (2003) 1509-1525.

[8.25] Shiotani, T., Fujii, K., Aoki, T., and Amou, K., 'Evaluation of progressive failure using AE sources and improved b-value on slope model tests', *Prog. Acoust. Emiss. V.* **VII**, 7 (1994) 529-534.

[8.26] Colombo, S., Forde, M.C., Main, I.G., and Shigeishi, M., Predicting the ultimate bending capacity of concrete beams from the "relaxation ratio" analysis of AE signals', *Constr. Build. Mater.* **19** (2005) 746-754.

[8.27] Ohtsu, M., Uchida, M., Okamoto, T., and Yuyama, S., 'Damage assessment of reinforced concrete beams qualified by acoustic emission', *ACI Structural J.* **99**(4) (2002) 411-417.

[8.28] Shiotani, T., Nakanishi, Y., Iwaki, K., Luo, X., and Haya, H., 'Evaluation of reinforcement in damaged railway concrete piles by means of acoustic emission'. *Journal of Acoustic Emission*, **23** (2005) 260-271.

[8.29] Shiotani, T., Nakanishi, Y., Luo, X., Haya, H., and Inaba, T., 'Damage evaluation for railway structures by means of acoustic emission', *Key Eng. Mater.*, **270-273** (2004) 1622-1630.

[8.30] Shiotani, T., and Aggelis D. G., 'Evaluation of repair effect for deteriorated concrete piers of intake dam using AE activity'. *Journal of Acoustic Emission* **25** (2007) 69-79.

[8.31] Shiotani, T., Ohtsu, M., and Ikeda, K., 'Detection and evaluation of AE waves due to rock deformation', *Constr. Build. Mater.* **15**(5-6) (2001) 235-246.

[8.32] T. Shiotani, 'Evaluation of long-term stability for rock slope by means of acoustic emission technique', *NDT & E International* **39**(3) (2006) 217-228.

[8.33] Mix, P. E., 'Acoustic emissions' in 'Introduction to Nondestructive Testing', Wiley, Hoboken, New Jersey, 2005.

[8.34] Kaiser. PhD Thesis, Technische Hochschule Munich; 1950.

[8.35] ASTM E569 - 07 Standard Practice for Acoustic Emission Monitoring of Structures During Controlled Stimulation (http://www.astm.org/Standards/E569.htm)

[8.36] Mindess S., 'Acoustic Emission Methods' in 'CRC Handbook of Nondestructive Testing of Concrete', Editors Malhotra V.M. and Carino N. J., (CRC, Boca Raton, Florida 2004).

[8.37] Matikas, T.E., 'Influence of material processing and interface on the fiber fragmentation process in titanium matrix composites', *Compos. Interfaces***15**(4) (2008) 363-377.

[8.38] Matikas, T.E., 'Analysis of load transfer behaviour and determination of interfacial shear strength in single-fibre-reinforced titanium alloys', *Advanced Composites Letters* **16**(5) (2007) 181-192.

[8.39] Waterbury, M.C., Karpur, P., Matikas, T.E., Krishnamurthy, S., and Miracle, D.B., 'In situ observation of the single-fiber fragmentation process in metal-matrix composites by ultrasonic imaging', *Compos. Sci. Tehcnol.* **52**(2) (1994) 261-266.

[8.40] Ohtsu, M., Tomoda, Y., 'Phenomenological model of corrosion process in reinforced concrete identified by acoustic emission', *ACI Mater J* **105**(2) (2007) 194–200.

[8.41] Aggelis D.G., Barkoula N.M., Matikas T.E., Paipetis A. S., 'Acoustic emission monitoring of degradation of cross ply laminates', *Journal of the Acoustical Society of America* 127(6) (2010) EL246-251.

[8.42] ASTM E2533 - 09 Standard Guide for Nondestructive Testing of Polymer Matrix Composites Used in Aerospace Applications.

[8.43] ASTM E569 - 07 Standard Practice for Acoustic Emission Monitoring of Structures During Controlled Stimulation.

[8.44] Mihashi, H., Nomura, N. and Niiseki, S., 'Influence of aggregate size on fracture process zone of concrete detected with three dimensional acoustic emission technique', *Cem. Concr. Res.* **21** (1991) 737-744.

[8.45] Shiotani, T., Nakanishi, Y., Luo, X. and Haya, H., 'Damage assessment in deteriorated railway sub-structures using AE technique', *Journal of Acoustic Emission* **22** (2004) 39-48.

[8.46] Colombo, S., Forde, M. C., Main, I. G., and Shigeishi, M., 'Predicting the Ultimate Bending Capacity of Concrete Beams from the 'Relaxation Ratio' Analysis of AE Signals', *Constr. Build. Mater.* **19** (2005) 746-754.

[8.47] Colombo, S., Main I.G., and Forde M.C., 'Assessing Damage of Reinforced Concrete Beam Using "b-value" Analysis of Acoustic Emission Signals', *J. Mater. Civ. Eng.* **15**(3) 2003 280-285.

[8.48] Shiotani, T., Luo, X. and Haya, H., 'Damage diagnosis of railway concrete structures by means of one-dimensional AE sources', *Journal of Acoustic Emission* **24** (2006) 205-214.

[8.49] Anastassopoulos A.A. and Philippidis T.P., 'Clustering Methodology for Evaluation of Acoustic Emission from Composites', *Journal of Acoustic Emission* **13**(1/2) (1994) 11-22.

[8.50] Soulioti, D., Barkoula, N.M., Paipetis, A., Matikas, T.E., Shiotani, T., Aggelis D.G., 'Acoustic emission behaviour of steel fibre reinforced concrete under bending', *Constr. Build. Mater.* **23** (2009) 3532-3536.

[8.51] Soulioti, D.V., Barkoula N.M., Paipetis, A., Matikas, T. E., 'Effects of fibre geometry and volume fraction on the flexural behaviour of steel-fibre reinforced concrete, Strain, (2010) in print.

[8.52] Aggelis, D.G., Polyzos, D. and Philippidis, T.P., 'Wave dispersion and attenuation in fresh mortar: theoretical predictions vs. experimental results', *J. Mech. Phys. Solids* **53**(4) (2005) 857-883.

[8.53] Cowan, M.L., Beaty, K., Page, J.H., Zhengyou, L., Sheng, P., 'Group velocity of acoustic waves in strongly scattering media: Dependence on the volume fraction of scatterers', *Physical Review E* **58**(5) (1998) 6626-6636.

[8.54] Wave2000, Cyber-Logic, Inc, NY (http://www.cyberlogic.org)

[8.55] Kaufman, J.J., Luo, G. and Siffert, R. S., 'Ultrasound Simulation in Bone,' *IEEE transactions on ultrasonics, ferroelectrics and frequency control* **55**(6) (2008) 1205-1218.

[8.56] Aggelis D.G. and Shiotani. T., 'Experimental study of surface wave propagation in strongly heterogeneous media', *Journal of the Acoustical Society of America* **122**(5) (2007) EL 151-157.

[8.57] Moser, F., Jacobs, L.J., Qu, J., 'Modeling Elastic Wave Propagation in Waveguides with Finite Element Method,' *NDT&E International*, 32 (1999) 225–34.